Letter

Nonthermal entanglement dynamics in a dipole-facilitated glassy model with disconnected subspaces

Guanhua Chen [1] and Yao Yao [1,2,*]

[1]*Department of Physics, South China University of Technology, Guangzhou 510640, China*

[2]*State Key Laboratory of Luminescent Materials and Devices, South China University of Technology, Guangzhou 510640, China*

(Received 22 March 2023; revised 31 July 2023; accepted 28 November 2023; published 18 January 2024)

We construct a dipole-facilitated kinetic constraint to partition the Hilbert space into three disconnected subspaces, two of which are nonthermal and the other acts as an intrinsic thermal bath. The resulting glassy system freely oscillates in nonthermal subspaces, making the quantum entanglement perform like a substantial qubit. The spatially spreading entanglement, quantified by concurrence, fidelity, and 2-Rényi entropy, is found to be spontaneously recovered, which is absent in other reference models. Under low-frequency random flip noise, this reversible hydrodynamics of entanglement holds high fidelity and volume law, while at high frequency thermalization unusually occurs leading to a strange phase transition. Our work offers an elaborate space structure for realizing ergodicity breaking and controllable entanglement dynamics.

DOI: 10.1103/PhysRevResearch.6.L012015

From the traditional thermodynamic perspective, entropy simply increases when more states in the Hilbert space are populated. Recent progress in random quantum circuits, however, indicates that measurement can induce breakdown of entropic volume law, as a unitary transformation makes the spreading entanglement entropy increase by 1 in each step, implying its particle nature [1,2]. It is then very interesting whether the entanglement can be manipulated as a substantial particle; but, just as in superconducing circuits [3,4], the uniform levels of the particle hinder efficient quantum control and it has to be reduced to two-level system enabled by specific anharmonicity. Subsequently, it serves as the main object of the present work to introduce well-designed kinetic constraints to disconnect the subspaces to which the entanglement may spread.

In glassy systems, kinetic constraints give rise to weak ergodic breaking in the presence of the fragmentation of Hilbert space with outlying nonthermal states [5–7]. For example, in a triangular antiferromagnetic lattice, the dynamics of a local spin is frustrated due to the constraint from neighboring spins [8,9]. In the spin glass phase, therefore, long-range orders are absent and the featured timescale of thermalization becomes ultraslow. This interesting local dynamics is then described by kinetically constrained models (KCMs), such as the Fredrickson-Andersen (FA) model and the East model [10–12]. Based on the disorder-free quantum East model, it has been proved that a large number of nonthermal states can be constructed to manifest area-law entanglement entropy [13,14]. In this Letter, we introduce a new dipole-facilitated kinetic constraint, which results in unusual ergodicity breaking by two disconnected subspaces. Initially from the Bell state and the Greenberger-Horne-Zeilinger (GHZ) state, we will study the exotic dynamics of entanglement within this elaborately constructed block structure of Hilbert space.

Our basic idea is to constrain the spin flip by some specific neighboring state, which is motivated by the CNOT gate in quantum computation with the control circuit being instead composed of two spins or a dipole. We start from cutting a triangular spin lattice into a quasi-one-dimensional chain as sketched in Fig. 1(a) [15,16]. Odd and even sites are separated into lower and upper sides labeled by different colors. The constraint rule is described as follows. First, two neighboring spins favor antiparallel configuration due to antiferromagnetic interaction. Second, a third spin in the triangle formed with these two spins is allowed to flip only if its neighboring spin is in the down state. Of course we can consider in parallel the constraint from the up state, but that is surely equivalent. This proposed KCM is named the dipole-facilitated model (DFM). The model Hamiltonian is written as

$$H_{\mathrm{df}} = \sum_{i=1}^{L} (Q_i P_{i+1} X_{i+2} + X_i P_{i+1} Q_{i+2}), \tag{1}$$

where X_i is the x-Pauli operator on ith site, $Q_i = |\uparrow\rangle\langle\uparrow|_i$, and $P_i = |\downarrow\rangle\langle\downarrow|_i$ are projectors of spin-up and spin-down, respectively. Throughout this work, the periodic boundary condition (PBC) is adopted for this model.

On the potential experimental realization of the model, we first notice that the Rydberg atoms, an ideal experimental platform for KCMs, have been used to study nonequilibrium and slow dynamics [17–19]. The excited and ground state of atom can be mapped as spin-up and-down. Under some controllable experimental conditions, the nearest-neighbor Rydberg blockade effect can be well described by the so-called PXP model [20,21], which has a very similar constraint with the present

*yaoyao2016@scut.edu.cn

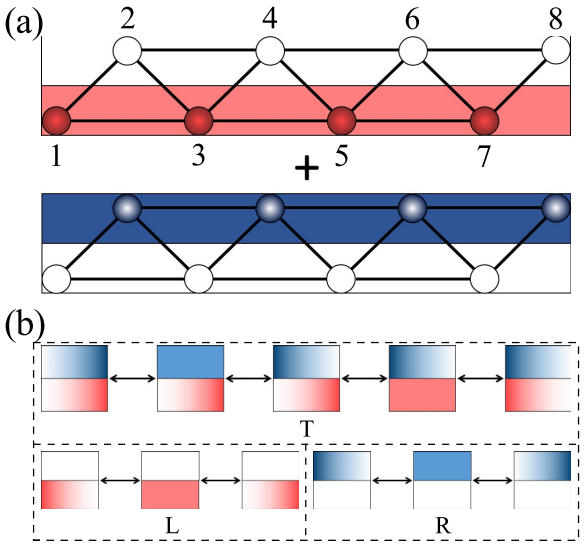

FIG. 1. (a) Schematic of an eight-site GHZ state with the circle representing that the site is in the spin-down state and the ball representing spin-up. Red and blue zones denote that the states of relevant sites are changeable. (b) A thermal subspace (T) and two nonthermal subspaces (L and R) are shown in disconnected block representation. The upper and lower halves in each square (solid: ↑↑; white: ↓↓; gradient: ↑ ↓ or ↓↑) represent even and odd sites, respectively.

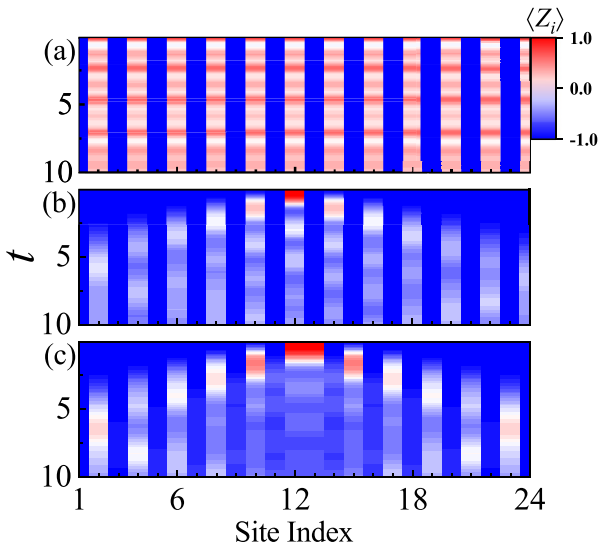

FIG. 2. Time evolution of $\langle Z_i \rangle$ on a 24-site lattice. (a) The initial state is $|\downarrow\uparrow\ldots\downarrow\uparrow\rangle$. The odd sites keep in spin-down and even sites behave periodic oscillation. (b) The initial state is $|\downarrow\ldots\downarrow\uparrow\downarrow\ldots\downarrow\rangle$, i.e. a single spin-up is located at $i = 12$, which spreads to the ends of the chain but odd sites keep in spin-down persistently. (c) The initial state is $|\downarrow\ldots\downarrow\uparrow\uparrow\downarrow\ldots\downarrow\rangle$, i.e. the $i = 12$ and 13 sites are in spin-up. Differently, spin-up states will cover all sites after sufficiently long time.

DFM. In this context, we think that the DFM should not be difficult to realize in a Rydberg atom array.

Let us first discuss the Hilbert space of DFM in block representation [22]. We consider four sites as an example. Two successive sites are grouped into one "group site," and we denote $(\downarrow\downarrow)$, $(\uparrow\downarrow)$, $(\downarrow\uparrow)$ and $(\uparrow\uparrow)$ as $\circ$, $\triangleright$, $\triangleleft$, and $\bullet$, respectively. Under the action of $H_{\rm df}$, we notice that the configurations $(\circ\circ)$, $(\triangleleft\triangleright)$, $(\triangleleft\bullet)$, $(\bullet\triangleright)$, and $(\bullet\bullet)$ are annihilated and the rest can be categorized into three subspaces. The transformation rules are

$$\begin{aligned} &\mathrm{T}: \circ\bullet \longleftrightarrow \triangleright\bullet \longleftrightarrow \triangleright\triangleleft \longleftrightarrow \bullet\triangleleft \longleftrightarrow \bullet\circ, \\ &\mathrm{L}: \circ\triangleright \longleftrightarrow \triangleright\triangleright \longleftrightarrow \triangleright\circ, \quad \mathrm{R}: \circ\triangleleft \longleftrightarrow \triangleleft\triangleleft \longleftrightarrow \triangleleft\circ . \end{aligned} \tag{2}$$

These three reaction paths can be straightforwardly extended to any longer chains and subsequently used to construct a large thermal subspace labeled by T and two nonthermal subspaces labeled by L (all even sites are spin-down) and R (all odd sites are spin-down), as sketched in Fig. 1(b).

Most interestingly, these three disconnected subspaces totally decide the active spatial state of systems. For example, if the initial state of a system without perturbation is $|\uparrow\downarrow\cdots\uparrow\downarrow\rangle$, even sites will persistently stay in spin-down state, implying that both the variational iteration for the ground state and the time evolution are confined to the subspace L. The reverse holds true as well, namely, states initiated from $|\downarrow\uparrow\cdots\downarrow\uparrow\rangle$ stay in the R subspace. Hence, the ground state with even number of sites possesses twofold degeneracy. It is worth noting that open chains with an odd number of sites also hold interesting topology, for instance the ground state of three sites gives $\frac{\sqrt{2}}{2}|\uparrow\downarrow\uparrow\rangle - \frac{1}{2}|\uparrow\downarrow\downarrow\rangle - \frac{1}{2}|\downarrow\downarrow\uparrow\rangle$. Now, if we have an initial state $|0\rangle = |\downarrow\downarrow\cdots\downarrow\downarrow\rangle$, it will evolve into a completely different subspace and stay there depending on how we add spin-up into the lattice. Adding a single spin-up to an even (odd) site activates the R (L) subspace, and two successive spin-ups break the confinement of above two nonthermal subspaces leading to the T subspace, which may act as an intrinsic thermal bath as discussed below.

One may ask if these disconnected subspaces possess features similar to that in the Hilbert space fragmentation. Breaking the Hilbert space into disconnected sectors is a nontrivial feature of generic KCM, but in most cases the number of Krylov subspaces is exponentially dependent on the system size [19]. In our DFM the number of subspaces is fixed no matter how large the system is, which is, as stated, essential to produce nontrivial entanglement dynamics.

In the following, we use time-evolving block decimation (TEBD) to compute the dynamics on the chain [23,24]. We first show the time evolution of the expectation value of the z-Pauli operator $\langle Z_i \rangle$ with different initial states for $L = 24$. Figures 2(a) and 2(b) show the results from the initial states $|\downarrow\uparrow\cdots\downarrow\uparrow\rangle$ and $|\downarrow\cdots\downarrow\uparrow\downarrow\cdots\downarrow\rangle$, respectively. In two cases, the spins are continuously flipped on the even sites, but all odd sites keep spin-down without any flipping. That is, the system freely oscillates in the R subspace resulting from ergodicity breaking. The parallel case in L subspace is not shown. For a comparison, we calculate the initial state with two successive spin-up sites in the middle of the chain, namely $|\downarrow\cdots\downarrow\uparrow\uparrow\downarrow\cdots\downarrow\rangle$ as shown in Fig. 2(c). This will transform the subspaces L and R to T and the system becomes ergodic, as all sites are being flipped in the time evolution.

Let us now categorize all sites into two for convenience with regard to quantum computations. The sites always being spin-down in a product state are called idle sites and the others work sites. For instance, in L subspace, all odd sites are work

and even sites are idle, and they are reversed in R subspace. As long as the system is sufficiently large, the probability that all work sites simultaneously flip to spin-down is extremely low. Therefore, we can denote idle sites as 0, work sites together as 1, to form a large and substantial logical qubit. In superconducting circuits, quantum nondemolition parity measurements can be realized by assigning some physical qubits as control nodes to detect errors of adjacent data qubits [25]. Analogously, herein, if we introduce a spin-up at a left end work site, the right end work site will tell us the initial odevity, and errors caused by noise can be detected by the appearance of successive spin-ups. It is remarkable that this transformation from nontrivial subspaces to T space is irreversible, and the system is unable to spontaneously evolve back to L or R subspace in the absence of other external fields. A single logical qubit can thus be in a superposition of product states in the L and R subspace, labeled by $|L\rangle$ or $|R\rangle$ respectively, paving a way for fault tolerance with this "big" qubit.

In order for our logical qubit to act as a quantum computing resource, we have to properly measure the correlation between two subspaces instead of two states, as well as the thermalization induced by a third large subspace. We notice that the spatial inversion symmetry is well reserved in the nonthermal subspaces, that is, the work sites in both subspaces can be paired and one-to-one mapped. The bipartite entanglement between these pairs of sites could thus feature the correlation between disconnected subspaces. Intuitively, the bipartite entanglement between two sites as a subsystem is affected by other sites, which may generate entanglement dissipation or disentanglement. Here, due to the absence of direct interaction between neighboring sites in nontrivial subspaces, this noiseless dynamics of the middle two sites can be actually characterized as the entanglement between subspaces L and R. To this end, we can operate a two-qubit gate to obtain an initial local Bell state ($L = 8$), i.e., $|\text{Bell}\rangle = \frac{1}{\sqrt{2}}(|\downarrow\downarrow\downarrow\downarrow\uparrow\downarrow\downarrow\downarrow\rangle + |\downarrow\downarrow\downarrow\uparrow\downarrow\downarrow\downarrow\downarrow\rangle)$, which will generally be evolving into $|L\rangle + |R\rangle$. We calculate the concurrence between middle two sites to quantize the bipartite entanglement [26,27], which is defined as

$$C(\rho) = \max\{\lambda_1 - \lambda_2 - \lambda_3 - \lambda_4, 0\}, \tag{3}$$

where λ_k's are the eigenvalues in descending order of the Hermitian matrix $r = \sqrt{\sqrt{\rho}\tilde{\rho}\sqrt{\rho}}$ and $\tilde{\rho} = (\sigma_y \otimes \sigma_y)\rho^*(\sigma_y \otimes \sigma_y)$. σ_y and ρ are y-Pauli matrix and reduced density matrix of the two middle sites by partially tracing others [28].

As displayed in Fig. 3(a), we observe a surprising periodicity of the entanglement, especially its maximum, which is very like a Newton's cradle. This nonthermal hydrodynamic behavior stems from two superposed bases of $|\text{Bell}\rangle$ being restricted in two disconnected nonthermal subspaces, and the time evolutions in these two subspaces are completely symmetric for spatial inversion, allowing the entanglement to be spontaneously recovered after spreading. In terms of this spatial inversion symmetry, three other initial entangled states breaking this symmetry are also calculated. It is clear that, although the maximum entanglements are different, all the features of time evolution are the same. Notice that the middle bipartite entanglement could be propagated from the other Bell pair of $|L\rangle + |R\rangle$. As illustrated by Fig. 3(b),

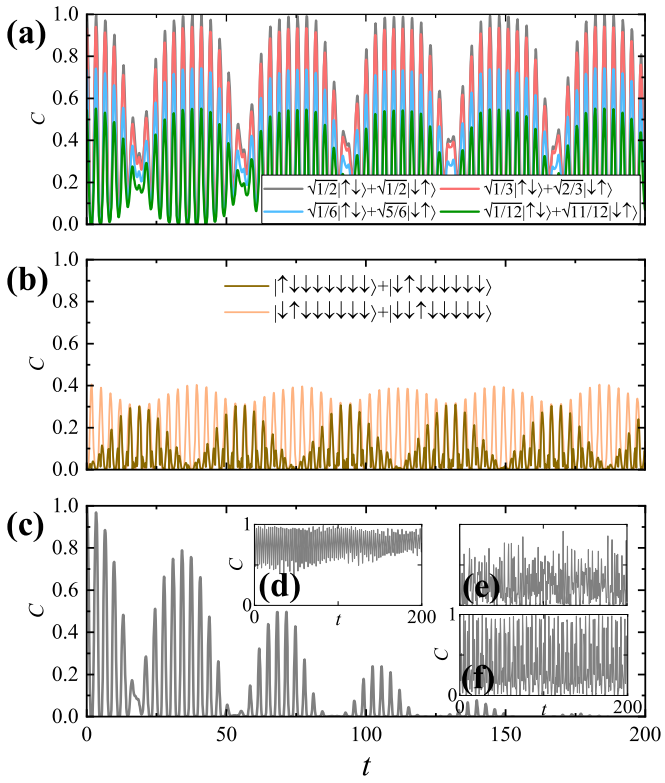

FIG. 3. Concurrence between the middle two sites ($i = 4$ and 5) in eight-site systems. (a) Time evolution with DFM shows recoverable periodic oscillations. Initially, the middle two sites are set with $\sqrt{1/2}|\uparrow\downarrow\rangle + \sqrt{1/2}|\downarrow\uparrow\rangle$ (black, the Bell state), $\sqrt{1/3}|\uparrow\downarrow\rangle + \sqrt{2/3}|\downarrow\uparrow\rangle$ (red), $\sqrt{1/6}|\uparrow\downarrow\rangle + \sqrt{5/6}|\downarrow\uparrow\rangle$ (blue), $\sqrt{1/12}|\uparrow\downarrow\rangle + \sqrt{11/12}|\downarrow\uparrow\rangle$ (green), and other sites are all in spin-down. Initial states in the following are all set as the Bell state. (b) The entangled Bell pairs of initial states are set to sites with $i = 1$ and $i = 2$ (brown), $i = 2$ and $i = 3$ (orange). (c) Adding a random flip noise with $T_X = 1$, the bipartite entanglement gradually decreases during oscillation. This calculation result is averaged over 1000 samples for random X operators. Insets are results of time evolution without noise under (d) the East model at the Rokhsar-Kivelson point, (e) the PXP model from the Rydberg blockade, and (f) the antiferromagnetic Heisenberg model, which do not show periodic behavior. The East model is in open boundary condition and others are in PBC.

the middle bond starts with $C = 0$ having the same wave packet period with that in (a), and a phase difference of π between two nearest neighboring sites is observed during the propagation. For comparison, three other typical models of spin chain are referenced, namely the East model, the PXP, model and the antiferromagnetic Heisenberg model as shown in Figs. 3(d)–3(f). There are no conserved quantities in the PXP model, which was first introduced in quantum many-body scars and also in the East model for describing spin glasses [14]. The Heisenberg model merely conserves the total spin. Remarkably, concurrences in these three models do not perform any visible cradlelike periodicity but just irregular oscillations.

We then mimic the inevitable noise, which can be described as (off-diagonal) bit flip and the (diagonal) projection, respectively. In the first case if an idle site is flipped from

spin-down to spin-up by off-diagonal noise, one of the subspaces L or R will be transferred into T. As a result, the entangled state is destroyed irreversibly by the T thermal bath, manifesting the usefulness of this intrinsic bath. We then add a random measurement into the Hamiltonian as a noisy source, following the form

$$H_{\mathrm{X}}(t) = H_{\mathrm{df}} + \sum_n X_j \delta(t - nT_{\mathrm{X}}), \tag{4}$$

where j is a random site to be periodically kicked every $t = nT_{\mathrm{X}}$. That is, at each time point nT_{X}, a Floquet operator $e^{i\varepsilon X_j}$ acts during the time step ε which is fixed to 0.1 in our simulation. Herein, the time step determines the strength of kicks, and increasing it apparently gives rise to quicker decoherence. Noting that, previous researches have found an emergent prethermal plateau and a many-body dynamically localized phase with Floquet kicking, which have been realized experimentally in a kicked dipolar model with nuclear magnetic resonance (NMR) techniques [29–31]. In Fig. 3(c), we observe, that although the concurrence still oscillates, the envelope decays gradually under the noise $T_{\mathrm{X}} = 1$ and will not recover, manifesting the irreversible breaking of periodicity. This so-called sudden death of concurrence and rebirth at short time implies a kick-induced phase transition [32,33]. That is, a random measurement transfers one idle site of a Bell state into the T subspace and the other remains in L or R, and there is definitely no entanglement when the state is superposed between T and L (R). Eventually, a few states in T can be transferred back to L or R leading to the rebirth, but in total the entanglement will quickly decay due to the largeness of T. In the case of diagonal noise, we can also set a noisy Hamiltonian similar to Eq. (4) with projectors Q_i or P_i, which are usually applied in a measurement-induced phase transition and have been experimentally realized on a superconducting quantum processor [34–36]. Compared with the off-diagonal noise which connects subspaces, these diagonal projectors do not hybridize the subspaces unless all work sites are simultaneously set to be 0, which is almost impossible, so their influence is much easier to eliminate and is not considered here.

As stated, the advantage of DFM turns out to be that we can use L and R subspaces as a logical qubit, so that we have to consider the entanglement not only between two sites but also between all odd and even sites, which is highly nontrivial as the contact area is no longer a single point such that the area-law entanglement has to be reconsidered. We then move on to consider the eight-site GHZ state $|\mathrm{GHZ}\rangle = \frac{1}{\sqrt{2}}(|\uparrow\downarrow\uparrow\downarrow\uparrow\downarrow\uparrow\downarrow\rangle + |\downarrow\uparrow\downarrow\uparrow\downarrow\uparrow\downarrow\uparrow\rangle)$ as the initial state, which also belongs to $|L\rangle + |R\rangle$ and has many-body entangled properties distinguished from the Bell state. We calculate the fidelity $F = |\langle \mathrm{GHZ}|\phi(t)\rangle|$ between an evolving and GHZ state to characterize the influence of actions under noise, which actually quantifies the fluctuation of the initial state. As shown in Fig. 4(a), for the system without random actions, the fidelity is able to come back to 1 periodically, implying perfect many-body revivals. By adding a noisy term, the fidelity is gradually decreasing over time, i.e., the distance between the evolving state and $|\mathrm{GHZ}\rangle$ is increasing.

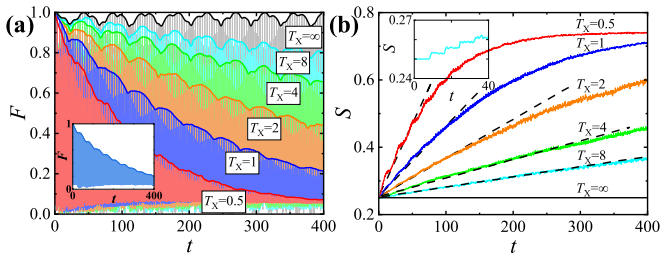

FIG. 4. Fidelity and reduced 2-Rényi entropy evolving with H_{X}. (a) The fidelity $F = |\langle \mathrm{GHZ}|\phi(t)\rangle|$ with $T_{\mathrm{X}} = 0.5$ (red), $T_{\mathrm{X}} = 1$ (blue), $T_{\mathrm{X}} = 2$ (orange), $T_{\mathrm{X}} = 4$ (green), $T_{\mathrm{X}} = 8$ (cyan), and $T_{\mathrm{X}} = \infty$ (black) is obtained after quench from eight-site $|\mathrm{GHZ}\rangle$. The system has high-frequency oscillation behavior, and the envelope lines of higher bounds are bolded. The $T_{\mathrm{X}} = \infty$ case is equal to evolution under H_{df}, which shows periodicity without decay. The inset shows the fidelity of the W state with $T_{\mathrm{X}} = 1$, holding explicitly the same features as the GHZ state. (b) The reduced 2-Rényi entropy $S(\rho)$ of even sites for different T_{X}. At $T_{\mathrm{X}} = \infty$, the entropy is constant over time. Dashed lines indicate the linear dependency of entropy and time, namely the volume law. The inset shows details of S for $T_{\mathrm{X}} = 8$ at short time. All results are averaged over 500 runs for X operators on random sites.

In addition to the GHZ state, we can also consider other many-body entangled states such as the W state, $|\mathrm{W}\rangle = \frac{1}{2\sqrt{2}}(|\uparrow\downarrow\downarrow\downarrow\downarrow\downarrow\downarrow\downarrow\rangle + |\downarrow\uparrow\downarrow\downarrow\downarrow\downarrow\downarrow\downarrow\rangle + \cdots)$. Interestingly, in the representation of subspaces, the W state can also be expressed as $|\mathrm{W}\rangle \Rightarrow |L\rangle + |R\rangle$ and we plot an instanced fidelity of $|\mathrm{W}\rangle$ in the inset of Fig. 4(a), showing features equivalent to the GHZ state. This suggests one of the most intriguing properties of DFM, that is, using a logical entangled state to denote certain different many-body entangled states.

The entanglement between odd and even sites has rarely been studied, but can provide more useful information than commonly using half-chain entanglement entropy. The reduced 2-Rényi entropy with a normalized logarithmic base for the reduced density matrix ρ of even sites is then defined as

$$S(\rho) = -\log_{16} \mathrm{Tr}(\rho^2), \tag{5}$$

which also characterizes the localization of the wave function [37]. As depicted in Fig. 4(b), without noise the entanglement remains a fixed value $S_{\min} = \log_{16} 2 = 0.25$, with respect to two nonzero diagonal elements in the reduced density matrix. In other cases, the Rényi entropy keeps growing before being saturated. There is a significant phase transition: For $T_{\mathrm{X}} > 1$ the entropy is in the early stage linearly dependent on time, suggesting that the system stays in an entangling phase with the volume law, and for $T_{\mathrm{X}} < 1$ the entropy rapidly saturates, indicating that the measurement induces an area-law disentangling phase and thermalization takes place instead of localization in common cases. More interestingly, since the contact area is now proportional to the chain length, the area-law entropy becomes even larger than the volume-law entropy. The inset of Fig. 4(b) shows notable platforms during entanglement evolution, revealing that each kick activates more states on the kicked sites, making those idle sites contribute to the contact area and resulting in sudden increase at $t = nT_{\mathrm{X}}$. We can thus explain the whole phenomenon like

this. In the small nonthermal subspaces the entanglement is periodic and localized so the increase is extremely slow, while when the localization is broken down, due to the contact being sufficiently broad, a large number of idle sites will instantly evolve into the large thermal T subspace to make the entropy rapidly increase. Consequently, the T subspace itself performs as an intrinsic thermal bath for nonthermal subspaces which is the most appealing structure of DFM.

In summary, originating from triangular frustrated kinetic constraints, the DFM manifests exotic disconnected subspace structure. The entanglement exhibits appealing nonthermal periodic dynamics acting as a substantial qubit. Under low-frequency flip noise, the entanglement ballistically increases while at high frequency it saturates in an instant, indicating that a phase transition to thermalization takes place stemming from the intrinsic thermal subspace. It should be noted that our model is closely related to the disorder-free localization model [38], which can be equivalent to the square of DFM on a triangle of the lattice.

The authors gratefully acknowledge support from the National Natural Science Foundation of China (Grants No. 11974118 and No. 12374107) and the Special Project for Research and Development in Key Areas of Guangdong Province (Grant No. 2020B0303300001).

[1] A. Nahum, J. Ruhman, S. Vijay, and J. Haah, Quantum entanglement growth under random unitary dynamics, Phys. Rev. X **7**, 031016 (2017).

[2] B. Skinner, J. Ruhman, and A. Nahum, Measurement-induced phase transitions in the dynamics of entanglement, Phys. Rev. X **9**, 031009 (2019).

[3] R. Barends, J. Kelly, A. Megrant, D. Sank, E. Jeffrey, Y. Chen, Y. Yin, B. Chiaro, J. Mutus, C. Neill, P. O'Malley, P. Roushan, J. Wenner, T. C. White, A. N. Cleland, and J. M. Martinis, Coherent josephson qubit suitable for scalable quantum integrated circuits, Phys. Rev. Lett. **111**, 080502 (2013).

[4] S. Kwon, A. Tomonaga, G. Lakshmi Bhai, S. J. Devitt, and J.-S. Tsai, Gate-based superconducting quantum computing, J. Appl. Phys. **129**, 041102 (2021).

[5] P. Sala, T. Rakovszky, R. Verresen, M. Knap, and F. Pollmann, Ergodicity breaking arising from Hilbert space fragmentation in dipole-conserving Hamiltonians, Phys. Rev. X **10**, 011047 (2020).

[6] S. Moudgalya and O. I. Motrunich, Hilbert space fragmentation and commutant algebras, Phys. Rev. X **12**, 011050 (2022).

[7] S. Moudgalya, B. A. Bernevig, and N. Regnault, Quantum many-body scars and Hilbert space fragmentation: a review of exact results, Rep. Prog. Phys. **85**, 086501 (2022).

[8] L. Balents, Spin liquids in frustrated magnets, Nature (London) **464**, 199 (2010).

[9] Y. Zhou, K. Kanoda, and T.-K. Ng, Quantum spin liquid states, Rev. Mod. Phys. **89**, 025003 (2017).

[10] F. Ritort and P. Sollich, Glassy dynamics of kinetically constrained models, Adv. Phys. **52**, 219 (2003).

[11] D. Chandler and J. P. Garrahan, Dynamics on the way to forming glass: Bubbles in space-time, Annu. Rev. Phys. Chem. **61**, 191 (2010).

[12] J. P. Garrahan, Aspects of non-equilibrium in classical and quantum systems: Slow relaxation and glasses, dynamical large deviations, quantum non-ergodicity, and open quantum dynamics, Physica A **504**, 130 (2018).

[13] M. van Horssen, E. Levi, and J. P. Garrahan, Dynamics of many-body localization in a translation-invariant quantum glass model, Phys. Rev. B **92**, 100305(R) (2015).

[14] N. Pancotti, G. Giudice, J. I. Cirac, J. P. Garrahan, and M. C. Bañuls, Quantum east model: Localization, nonthermal eigenstates, and slow dynamics, Phys. Rev. X **10**, 021051 (2020).

[15] T. Mishra, S. Greschner, and L. Santos, Polar molecules in frustrated triangular ladders, Phys. Rev. A **91**, 043614 (2015).

[16] T. Mishra, S. Greschner, and L. Santos, Frustration-induced supersolids in the absence of intersite interactions, Phys. Rev. B **92**, 195149 (2015).

[17] H. Bernien, S. Schwartz, A. Keesling, H. Levine, A. Omran, H. Pichler, S. Choi, A. S. Zibrov, M. Endres, M. Greiner *et al.*, Probing many-body dynamics on a 51-atom quantum simulator, Nature (London) **551**, 579 (2017).

[18] M. Ostmann, M. Marcuzzi, J. P. Garrahan, and I. Lesanovsky, Localization in spin chains with facilitation constraints and disordered interactions, Phys. Rev. A **99**, 060101(R) (2019).

[19] M. Magoni, P. P. Mazza, and I. Lesanovsky, Emergent bloch oscillations in a kinetically constrained Rydberg spin lattice, Phys. Rev. Lett. **126**, 103002 (2021).

[20] C. J. Turner, A. A. Michailidis, D. A. Abanin, M. Serbyn, and Z. Papić, Weak ergodicity breaking from quantum many-body scars, Nat. Phys. **14**, 745 (2018).

[21] C. J. Turner, A. A. Michailidis, D. A. Abanin, M. Serbyn, and Z. Papić, Quantum scarred eigenstates in a Rydberg atom chain: Entanglement, breakdown of thermalization, and stability to perturbations, Phys. Rev. B **98**, 155134 (2018).

[22] C.-J. Lin and O. I. Motrunich, Exact quantum many-body scar states in the Rydberg-blockaded atom chain, Phys. Rev. Lett. **122**, 173401 (2019).

[23] G. Vidal, Classical simulation of infinite-size quantum lattice systems in one spatial dimension, Phys. Rev. Lett. **98**, 070201 (2007).

[24] M. Fishman, S. R. White, and E. M. Stoudenmire, The ITensor software library for tensor network calculations, SciPost Phys. Codebases **4** (2022).

[25] J. Kelly, R. Barends, A. G. Fowler, A. Megrant, E. Jeffrey, T. C. White, D. Sank, J. Y. Mutus, B. Campbell, Y. Chen *et al.*, State preservation by repetitive error detection in a superconducting quantum circuit, Nature (London) **519**, 66 (2015).

[26] P. Horodecki, Measuring quantum entanglement without prior state reconstruction, Phys. Rev. Lett. **90**, 167901 (2003).

[27] L. Amico, R. Fazio, A. Osterloh, and V. Vedral, Entanglement in many-body systems, Rev. Mod. Phys. **80**, 517 (2008).

[28] A. Hamma, R. Ionicioiu, and P. Zanardi, Bipartite entanglement and entropic boundary law in lattice spin systems, Phys. Rev. A **71**, 022315 (2005).

[29] C. Fleckenstein and M. Bukov, Thermalization and prethermalization in periodically kicked quantum spin chains, Phys. Rev. B **103**, 144307 (2021).

[30] M. Fava, R. Fazio, and A. Russomanno, Many-body dynamical localization in the kicked Bose-Hubbard chain, Phys. Rev. B **101**, 064302 (2020).

[31] X. Huang, C. Ramanathan, P. Cappellaro, P. Peng, and C. Yin, Floquet prethermalization in dipolar spin chains, Nat. Phys. **17**, 444 (2021).

[32] T. Yu and J. H. Eberly, Sudden death of entanglement, Science **323**, 598 (2009).

[33] C. E. López, G. Romero, F. Lastra, E. Solano, and J. C. Retamal, Sudden birth versus sudden death of entanglement in multipartite systems, Phys. Rev. Lett. **101**, 080503 (2008).

[34] Q. Tang and W. Zhu, Measurement-induced phase transition: A case study in the nonintegrable model by density-matrix renormalization group calculations, Phys. Rev. Res. **2**, 013022 (2020).

[35] X. Turkeshi, A. Biella, R. Fazio, M. Dalmonte, and M. Schiró, Measurement-induced entanglement transitions in the quantum Ising chain: From infinite to zero clicks, Phys. Rev. B **103**, 224210 (2021).

[36] J. M. Koh, S.-N. Sun, M. Motta, and A. J. Minnich, Measurement-induced entanglement phase transition on a superconducting quantum processor with mid-circuit readout, Nat. Phys. **19**, 1314 (2023).

[37] R. Horodecki, P. Horodecki, M. Horodecki, and K. Horodecki, Quantum entanglement, Rev. Mod. Phys. **81**, 865 (2009).

[38] A. Smith, J. Knolle, D. L. Kovrizhin, and R. Moessner, Disorder-free localization, Phys. Rev. Lett. **118**, 266601 (2017).